

Metastable Helium Density Simulation and Discussion on the Observation Location of Lidar

Zhenwei Liu^(a), Xianghui Xue^(a*), Ruocan Zhao^(a)

(a) School of Earth and Space Sciences, University of Science and Technology of China
No 96, Jinzhai road, Hefei, Anhui, China

*Correspondence: xuexh@ustc.edu.cn

Abstract: The observation of metastable helium He(2³S) by ground-based resonant lidar has been gradually developing. For example, a corresponding lidar has been built in Danzhou, China, and has been observed for several months. More observations may be conducted in the future. So the paper will analyze the advantages and disadvantages of observations at different locations on Earth from the perspective of He(2³S) density, mainly using previously generation models of He(2³S) density and empirical models of energetic electron (>19.8eV) flux in polar regions. The results show that compared to passive observation conjugate photoelectrons have a significant impact on the observable duration of middle-low latitudes, and the precipitation electrons in polar regions are the main source of He(2³S) generation during most nights.

1. Introduction

The sharp enhancement near 1083 nm was first observed during the intense sunlit aurora on February 10-11, 1958 [1]. Over the past few decades, many observations of the 1083 nm emission intensity have been made at various magnetic latitudes [2,3]. In 1996, metastable helium spectral lines could be separated from hydroxyl groups [4], and in 1997, laser radar was proposed to observe metastable helium to obtain its height profile[5]. At the same time, the metastable helium density model is also constantly evolving, which is of great significance for understanding photoelectrons and monitoring the thermosphere atmosphere[6,7].

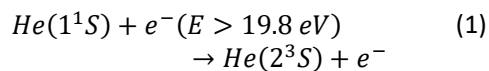
Due to the lack of density profile information, the model cannot be further improved. Recently, the He(2³S) density observation with lidar has been developed gradually, which can get He(2³S) density profile [8]. This helps to update the model and gain a better understanding of photoelectrons, thermosphere models, and more [6,7,9]. In order to provide more reference for lidar observations, this paper simulated the annual variation of He(2³S) concentration to better analyze the suitable observation periods for different observation locations.

The research describes the modeling process of the He(2³S) density model in the thermosphere (Section 2), which has made slight changes in the photoelectronic model compared to the previous He(2³S) model [10]. Then, density simulation results at low and high latitudes were presented based on this model, and the influence of polar precipitation electrons on He(2³S) density was discussed [8,10]. Section 4 discusses possible updates to metastable helium density models if future and possible phenomena at different observation locations.

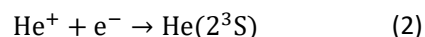
2. He(2³S) Density Model

The metastable helium density model in this paper is a single column, single time model.

The main generation mechanism of He(2³S) is the collision between ground state helium and energetic electrons (E>19.8 eV) by



The secondary generation mechanism is the recombination of helium ions with electrons:



So the He(2³S) excitation rate is calculated by

$$q(z) = q_e(z) + q_r(z) \quad (3)$$

$q_e(z)$ is the main generation rate:

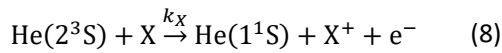
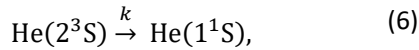
$$q_e(z) = \sum_E \Phi_e(z, E) \cdot \sigma(E) \cdot n[\text{He}(1^1)](z) \quad (4)$$

where $\sigma(E)$ is the electron collision cross section, $\Phi_e(z, E)$ is the photoelectron flux calculated based on the GLOW model, $n[\text{He}(1^1S)](z)$ is the density profile of ground state helium from the United States Naval Research Laboratory Mass Spectrometer and Incoherent Scatter Radar Exosphere (NRLMSISE-00). $q_r(z)$ is the secondary generation rate:

$$q_r(z) = \alpha_r [T_e(z)] \cdot n[\text{He}^+](z) \cdot n[e^-](z), \quad (5)$$

where $\alpha_r [T_e(z)]$ is the recombination coefficient. $n[\text{He}^+](z)$ is the density profile of helium ions from the IRI model. $n[e^-](z)$ is the electron density profile from the IRI model.

$\text{He}(2^3S)$ is lost mainly through radiation decay, photoionization, and Penning ionization.



Equation (6) is radiation decay with reaction rate coefficients $k = 1.1 \times 10^{-4} \text{ s}^{-1}$ [11]. Equation (7) is photoionization with reaction rate coefficients $J = 1.9 \times 10^{-3} \text{ s}^{-1}$ [12]. Equation (8) is Penning ionization through collision with molecules X (N_2 , O_2 and O) in the atmosphere. Its reaction rate coefficients is $k_{N_2} = 1.9 \times 10^{-9} \exp(-1.04 - 685/T) \text{ cm}^{-3} \text{ s}^{-1}$ [13], $k_{O_2} = 1.9 \times 10^{-9} \exp(-0.63 - 418/T) \text{ cm}^{-3} \text{ s}^{-1}$ [13], and $k_O = 1.034 \times 10^{-9} (T/150)^{1/6} \text{ cm}^{-3} \text{ s}^{-1}$ [14] respectively.

Based on the continuity equation, the diffusion equation is

$$\frac{d}{dz} \left[-D \left(\frac{dn}{dz} + \frac{n}{H} \right) \right] + Ln = q \quad (9)$$

where L is the total loss rate per atom, H is the scale height of the $\text{He}(2^3S)$ number density, D is the diffusion coefficient. The diffusion coefficient is calculated by

$$D = \left(\frac{n_{\text{He}}}{b_{\text{He}}} + \frac{n_O}{b_O} \right)^{-1} \quad (10)$$

where $b_{\text{He},O}$ are the binary collision coefficients of $\text{He}(2^3S)$ through atomic helium and atomic oxygen, respectively. $b_{\text{He}} = 9 \times 10^{17} T^{0.5}$ comes from theoretical calculations, while $b_O = 3 \times 10^{18} T^{0.5}$ comes from values obtained by fitting to the case.

The solar EUV (0.5-1750 Å) flux is determined by the EUVAC model (Richards et al. 1994), which is also described in the GLOW model [9]. The UV-related scaling factors used in the GLOW model are scaling switch ISCALE=1 and enhancement factor XUVFAC=3.

3. Results

The second phase of the Chinese Meridian Project is deploy $\text{He}(2^3S)$ lidar in Danzhou Hainan Province, so low latitude areas have been selected for modeling. The simulation results of the annual and LT variations in state helium density and the 1083 nm airglow intensity at 450 km in Danzhou are given in Figure 1. Combined with the annual and LT variations in the ground state helium from NRLESIS00 above, the annual variation in the $\text{He}(2^3S)$ column density can be roughly seen.

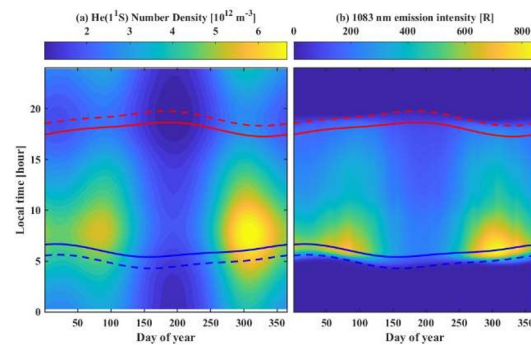


Figure 1. Seasonal and LT variations in (a) helium number density at 450 km and (b) 1083 nm emission intensity at Danzhou, Hainan.

The blue line represents dawn, the red line represents dusk, the solid line indicates that the solar zenith angle is 90° , and the dotted line indicates that the solar zenith angle is 104° .

The SZA corresponding to $\lambda=30.4$ nm solar ultraviolet screening height (i.e., approximately 300 km[15]) is approximately 104° .

A radiation intensity of 1083 nm of approximately 10-12 R can be observed during polar sunlit auroras. This result is mainly because the precipitating electrons greatly enhance the $\text{He}(2^3S)$ density during aurora, but the influence of precipitating electrons on

He(2^3S) was not considered in the polar simulation below in order to understand the influence of photoelectrons.

First, the He(2^3S) column density in the polar region is simulated without precipitating electrons, as shown in Figure 2. In addition, the effect of conjugated photoelectrons on local photoelectrons can be ignored due to photoelectron energy loss and pitch angle redistribution. Figure 2a shows the annual variation and LT variation in the ground state helium density at 450 km based on the NRLMSISE00 atmospheric model. The red solid line in the top half of the figure corresponds to the sunset time, and the blue solid line in the bottom half of the figure corresponds to the sunrise time. The middle of the two solid lines represents the day side, and the two sides represent the night side. As shown in Figure 2, the ground state helium density during the polar night is significantly larger than that during the polar day. As seen from Figure 2, the ground state helium density near the twilight lines is higher on the night side than the other and is higher at noon than for the rest of the day.

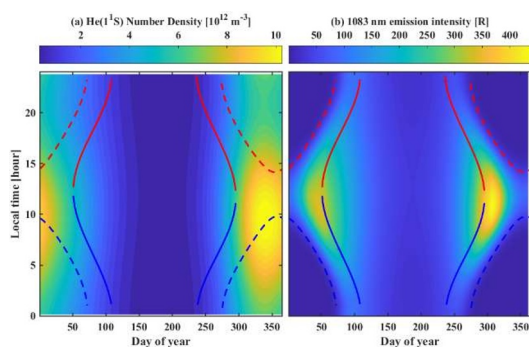


Figure 2. Seasonal and LT variations in (a) helium at 450 km and (b) 1083 nm emission intensity at the Chinese Yellow River Station.

The blue line represents dawn, the red line represents dusk, the solid line represents the SZA of 90° , and the dotted line represents the SZA of 104° .

Figure 3 shows the influence of precipitation electrons on the He(2^3S) density under different solar zenith angles. A very long continuous observation window is provided in the polar region, combined with the simulation of the annual variation of He(2^3S) density in the polar region in the paper (Figure 3).

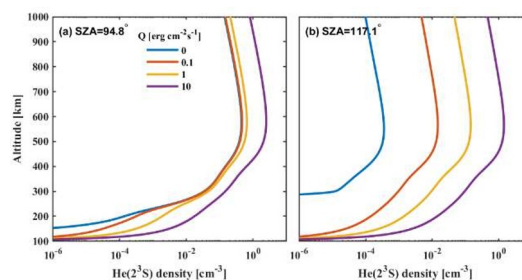


Figure 3. The influence of precipitation electrons

4. Conclusion and Discussion

Figure 4 shows the relative relationship between the magnetic field line and the twilight line. The transport effect of photoelectrons along the magnetic field line at the conjugate point will prolong the suitable observation time, which can also be seen from the simulation of the annual variation of He(2^3S) density in the paper.

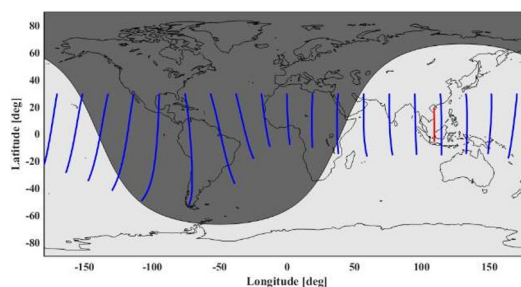


Figure 4. Schematic diagram of magnetic lines

Passive observation limits longer observation due to the limitation of sunlight, while lidar expands observation time, which may lead to new discoveries. For example, the longer lifetime of metastable helium may lead to the existence of metastable helium even after the disappearance of photoelectrons; The effect of magnetic field lines at lower latitudes and heights transporting photoelectrons leads to height changes in metastable helium; In polar regions, it can also be used to reflect the distribution of deposited electrons, and so on.

If more observational data is available, the impact of magnetic storms and winds on the distribution of metastable helium density can also be discussed in the model.

5. Acknowledgements

This work is supported by Key-Area Research and Development Program of Guangdong Province 2020B0303020001, Ground-based

Space Environment Monitoring Network (the Chinese Meridian Project), National Natural Science Foundation of China (Grant No42374185), and the Fundamental Research Funds for the Central Universities.

6. References

- [1] A. V. Mironov, Prokudina, V. S. & Shefov, N. N., "Observation of the aurora over Moscow on February 10–11, 1958 (in Russian)," Spectral, Electrophotometrical, and Radar Studies of Aurorae and Airglow, 20-24 (1959)
- [2] A. B. Christensen, T. N. Patterson, B. A. Tinsley, "Observations and Computations of Twilight Helium 10,830-Angstrom Emission," Journal of Geophysical Research **76**, 1764-+ (1971)
- [3] B. A. Tinsley, A. B. Christensen, "Twilight helium 10,830-Å calculations and observations," J. Geophys. Res-Space Phys. **81**, 1253-1263 (1976)
- [4] R. B. Kerr, J. Noto, R. S. Lancaster, M. Franco, R. J. Rudy, R. Williams, J. H. Hecht, "Fabry Perot observations of helium 10830 angstrom emission at Millstone Hill," Geophysical Research Letters **23**, 3239-3242 (1996)
- [5] A. J. Gerrard, T. J. Kane, D. D. Meisel, J. P. Thayer, R. B. Kerr, "Investigation of a resonance Lidar for measurement of thermospheric metastable helium," J. Atmos. Sol.-Terr. Phys. **59**, 2023-2035 (1997)
- [6] J. Bishop, R. Link, "He (23 S) densities in the upper thermosphere: Updates in modeling capabilities and comparisons with midlatitude observations," Journal of Geophysical Research: Space Physics **104**, 17157-17172 (1999)
- [7] J. Bishop, R. Link, "Metastable He 1083 nm intensities in the twilight: a reconsideration," Geophysical research letters **20**, 1027-1030 (1993)
- [8] B. Kaifler, C. Geach, H. C. Büdenbender, A. Mezger, M. Rapp, "Measurements of metastable helium in Earth's atmosphere by resonance lidar," Nat. Commun. **13**, 7 (2022)
- [9] S. C. Solomon, "Global modeling of thermospheric airglow in the far ultraviolet," Journal of Geophysical Research: Space Physics **122**, 7834-7848 (2017)
- [10] L. S. Waldrop, R. B. Kerr, S. A. González, M. P. Sulzer, J. Noto, F. Kamalabadi, "Generation of metastable helium and the 1083 nm emission in the upper thermosphere -: art. no. A08304," J. Geophys. Res-Space Phys. **110**, 12 (2005)
- [11] J. R. Woodworth, H. W. Moos, "Experimental determination of the single-photon transition rate between the 2 S 1 3 and 1 S 0 1 states of He i," Physical Review A **12**, 2455 (1975)
- [12] R. Stebbings, F. Dunning, F. Tittel, R. Rundel, "Photoionization of helium metastable atoms near threshold," Physical Review Letters **30**, 815 (1973)
- [13] W. Lindinger, A. Schmeltekopf, F. Fehsenfeld, "Temperature dependence of de - excitation rate constants of He (23 S) by Ne, Ar, Xe, H2, N2, O2, NH3, and CO2," The Journal of Chemical Physics **61**, 2890-2895 (1974)
- [14] R. D. Rundel, R. F. Stebbings, "Metastable helium in the Earth's upper atmosphere," Journal of Geophysical Research Atmospheres **79**, 681-684 (1974)
- [15] N. Shefov, A. Semenov, O. Yurchenko, "Empirical model of variations in the helium 1083 nm emission. 1. Intensity," Geomagnetism and Aeronomy **49**, 93-103 (2009)